Simple, Low-Cost Fabrication of Soft Sensors for Shape Reconstruction

Danna Ma, Steven Ceron, Gregory Kaiser, and Kirstin Petersen

***Abstract*—Shape reconstruction by soft sensors may be useful in applications ranging from precision agriculture to haptics and factory automation due to the potential for low-cost fabrication, durable operation, and safe and compliant interaction. Current prevalent techniques, however, require expertise, expensive materials, and high-end processing equipment which limits both their transition to practice and their accessibility to researchers. To address this issue, we present easily accessible, low-cost, and rapid fabrication techniques for soft and resistive carbon composite sensors. We characterize their repeatability and durability in response to stretch up to 135%. We further show how this fabrication technique may be easily customized to two different applications, including a stretchable, tactile interface for passive sensing, and an active, soft pneumatic gripper that can fully encompass an object to reconstruct its shape. We complement these with simple control and analysis, and show how to achieve high relative accuracy, despite the high manufacturing tolerances of the sensors.**

***Index Terms*—Soft sensors and actuators, soft robot materials and design.**

I. Introduction

SOFT sensors are an active area of research with diverse applications, many of which require repeatable interactions with fragile and irregular objects [1]. This has prompted demonstrations of materials with mechanical, chemical, and electrical response to changes in stretch, pressure and temperature [2] in search of durable, compliant and highly stretchable sensors. Materials like, e.g., polydimethylsiloxane [3] and silicone elastomers [4] have become popular choices, and a variety of fabrication techniques such as micro- and nano-contact patterning [5] and passivation techniques [6] are often applied to synthesize novel robotic sensors. The majority of these techniques, however, require prior knowledge and experience, which raises the barrier of entry to the field. To enable a greater number of researchers to customize soft sensors for their respective applications, it is important to minimize the cost of sensors and introduce fast, easily accessible fabrication.

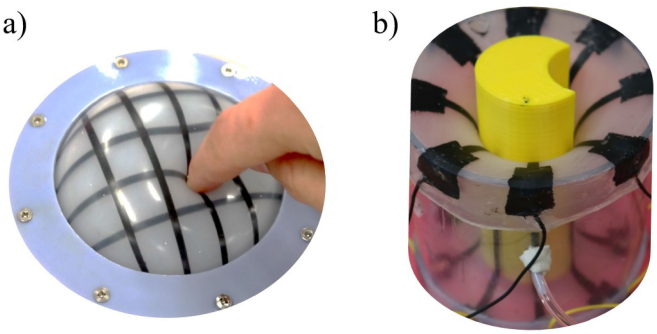

Fig. 1. We aim to lower the barrier of entry to soft sensors through simple fabrication, control, and data processing. We demonstrate our concept in two devices: (a) a tactile interface for contact sensing, and (b) a sensitive, pneumatic gripper which can estimate the 2D shape of an encompassed object.

Towards this end, we present a soft, low-cost sensor with a simple fabrication procedure that has high manufacturing tolerances; requires no advanced equipment, control sequences, or data processing; and can easily be customized for various applications.

We show that a specific ratio of inexpensive carbon black mixed by hand with an uncured silicone elastomer enables conductivity at high stretch. Furthermore, this gel has a high viscocity and is less prone to leakage compared to other popular conductive fluids such as Eutectic Gallium-Indium (EGaIn) [7]. We show how sensors using this composite can be made by non-experts in hours without expensive equipment. We demonstrate the customizability of the sensors through two devices: a passive sensor capable of detecting touch on the surface of an inflated membrane, as well as a sensitive pneumatic gripper that can encapsulate an object and stretch around its convex and concave features (Fig. 1). Using the latter, we show that object geometry can be estimated using a simple control sequence based on constant rate of inflation. To avoid issues with material buckling, we operate the gripper primarily in negative pressure such that the material is always experiencing stretch. Finally, despite the differences in the individual sensors, we further show that we can estimate the object shape, simply by normalizing the sensor response and identifying when the channels come into contact with the encompassed object.

Specifically, this paper presents the following contributions: 1) a widely accessible and low-cost fabrication procedure for a stretchable strain sensor composed of a carbon conductive

Manuscript received October 15, 2019; accepted March 12, 2020. Date of publication April 15, 2020; date of current version May 4, 2020. This letter was recommended for publication by Associate Editor Prof. Robert MacCurdy and Editor Kyu-Jin Cho upon evaluation of the reviewers' comments. This work was supported in part by the NSF: GRFP, in part by USDA-NIFA Cyber-Physical Systems Program under Award No. #2018-09054, and in part by the USDA-NIFA Hatch Fund #1014705. *(Corresponding author: Danna Ma.)*

Danna Ma and Kirstin Petersen are with the School of Electrical and Computer Engineering, Cornell University, Ithaca, NY 14853 USA (e-mail: dm797@cornell.edu; kirstin@cornell.edu).

Steven Ceron is with the Sibley School of Mechanical and Aerospace Engineering, Cornell University, Ithaca, NY 14853 USA (e-mail: sc2775@cornell.edu).

Gregory Kaiser is with the School of Applied and Engineering Physics, Cornell University, Ithaca, NY 14853 USA (e-mail: ghk48@cornell.edu).

Digital Object Identifier 10.1109/LRA.2020.2986746

filler embedded in a soft elastomeric matrix (Sec. II); 2) characterization of the durability of sensor over the course of 15 days and repeatability over the course of 30 inflation cycles; 3) demonstration of a dynamic, soft tactile grid with multiple sensor channels (Sec. III); 4) demonstration of 2D convex and concave shape reconstruction using a soft encompassing sensor, operating in negative and positive pressure with a simple control procedure (Sec. IV); and 5) a simple computational method for shape reconstruction that overcomes the individual differences between the low cost sensors. Through this work, we hope to make soft sensors and robots more widely accessible, enabling deployment in a broad range of applications.

II. Fabrication and Sensor Characterization

The following sections describe the design and fabrication procedures for the conductive composite and a single stretchable sensor. We further discuss two characterization tests of a sensor to demonstrate its resistive response to stretch.

A. Carbon Black Composite Preparation

Consumer demand is driving research to combine the flexibility of silicone materials and electrical properties of conductive filler materials for a variety of applications [8]. Silicone rubbers have great elongation and tensile strength, and offer good resistance to humidity and temperature. However, like most polymers, they are electrically insulating at low voltage due to the nonavailability of delocalized electrons. The majority of conductive composites are produced by adding conductive fillers, such as carbon black [9], carbon nanoparticles[10] and nanotubes [11], graphene sheets [12], graphene nanoplates [13] and silver nanoparticles [11].

One of the factors that determines a composite's conductivity and the percolation threshold is the concentration of the added conductive filler [9]. For expensive fillers such as silver nanoparticles and carbon nanotubes, concentrations that reach the percolation threshold are costly. In addition, achieving a homogeneous and stable dispersion of the filler is crucial to create the network for electrical transfer, and usually requires a polar aprotic solvent to assist the dispersion [14]. A variety of dispersion methods [9] and dispersing solvents have been developed [15] to improve this process. Unfortunately, these techniques can be time consuming and require expensive and high precision tools such as a ultrasonication bath and the Haake torque rheometer.

To address these issues, we demonstrate a fast, simple, accessible, and inexpensive fabrication technique which yields adequate conductivity for stretch up to 135%. To lower cost, we chose to disperse low grade carbon black into Ecoflex 00-30 Part A, and embed it into a support material of cured Ecoflex 00–10. Such carbon composites have previously been demonstrated to have high conductivity at up to 500% stretch [16]. Because the conductive gel is not cured, it is possible that Ecoflex silicone with a different shore hardness would work equally well. We conducted a pilot experiment with a carbon black powder (VULCAN XC72R) to Ecoflex mass ratio of 1:7 based on the electrical conductivity reported in [17]. We mixed the carbon black powder into Ecoflex 00-30 Part A with ethyl acetate as the dispersing agent. To further aid the dispersion of conductive carbon black powder, we applied $\sim$3 hours of continuous stirring at 100 rpm. No additional step is needed to remove the residual dispersing agent from the composite due to the low boiling point of ethyl acetate of 77.1 . To give an example, a volume of our composite the size of a quarter US coin costs 0.145 USD, as compared to 44.64 USD using EGaIn. Although EGaIn is a liquid metal at room temperature and can be used in smaller quantities which lowers the cost of the sensor, our technique is inexpensive, fast, leak-proof, and requires no prior training because operating high-precision equipment is not needed.

In pursuit of an even simpler and faster fabrication technique, we eliminated the use of the dispersing solvent and compensated by increasing the filler concentration. We increased the carbon black to Ecoflex ratio to 1:6 and mixed it by hand for several minutes. Doing this resulted in an uncured conductive gel that can be spread onto a polymer surface in a thin layer, as discussed in Sec. II-B. The cost of making a quarter coin-sized conductive composite with this technique is only 0.12 USD, saving an additional 18% compared to the pilot experiment. This simplified conductive composite fabrication technique requires no specialized equipment, takes only a few minutes, and is orders of magnitude faster than other common approaches.

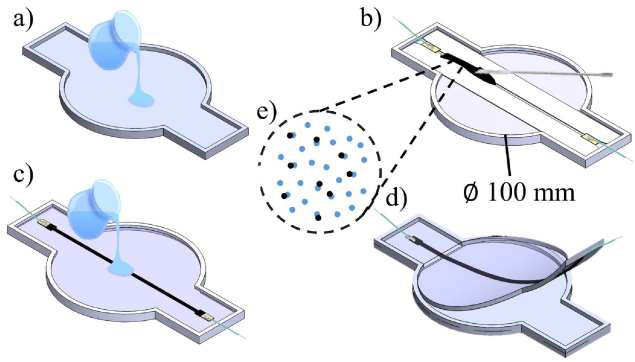

Fig. 2. Fabrication of a single sensor: (a) 15 g of Ecoflex 00–10 mixture is poured into a mold to form a layer of 1 mm thickness. (b) The cured Ecoflex is covered with a mask and the Carbon Black composite is spread across the channel. (c) The mask is peeled off leaving a conductive sensor channel and a second layer of 10 g of Ecoflex 00–10 mixture is poured. (d) The membrane is slowly peeled from the mold. (e) The carbon composite is composed of a 1:6 mass ratio of Carbon Black powder to Ecoflex 00–30.

B. Single Sensor Fabrication

Fig. 2 shows the process for embedding the carbon composite in Ecoflex gel to fabricate single sensors. First, we pour a 1 mm thick base layer Ecoflex rubber mixed 1A:1B by weight into a mold. To eliminate entrapped air, we vacuum degas the mixture before pouring. We cure the silicone for approximately 2 hours at room temperature, or speed up the process by using an oven at 70° C. After the silicone has cured, we cover it with a laser-cut stencil which is 0.8 mm in thickness. The stencil is 2 mm wide and corresponds to the width of the sensor. Note that the laser cutter was used for ease, but this stencil could easily have been cut by hand given its dimensions. Two copper electrodes

(20 mm × 5 mm) with wire leads are glued onto the base layer at the ends of the stencil using Sil-Poxy silicone adhesive. Next, using a micro-spatula, the conductive composite is spread over the stencil, connecting to the copper electrodes. The stencil is then peeled off and another layer of 1 mm thick Ecoflex rubber is poured on top. The end product is a single channel of conductive composite embedded in translucent support material. The entire fabrication process can be finished without the use of expensive equipment or advanced tools in less than 5 hours; 4 of which are curing time. Note that since the polymer is cured in a shallow mold, the vacuum chamber step can be skipped by simply pouring the silicone in a thin layer and popping remaining bubbles by hand with a sharp instrument.

C. Sensor Characterization

To demonstrate the robustness of the sensor, we first characterize its durability by inflating it once per day for 15 days, and then its repeatability over 30 inflation cycles. Both properties are important to long-term operation of the sensors which is critical in many applications.

The experimental setup for the sensor characterization tests is shown in Fig. 3(a-c). We characterized the single sensor by placing it under a circular clamp with a diameter of 85 mm and inflating it into a dome structure at approximately 50mL/s. We inflate the membrane for 2 s, hold the pressure for 5 s, and then deflate at the same rate for 2 s. We then wrote a Matlab-program to automatically extract the outline of the inflating dome and in turn, the strain experienced by the sensor during inflation and deflation. The stretch of the membrane is calculated by dividing the length of the outline of the inflated dome over the initial length of the membrane, which peaks at 135%. The sensor responses were normalized by subtracting and dividing by the initial resistance value recorded before actuation, i.e. while the sensor is not pressurized and not experiencing stretch.

In Fig. 3(d), we show the sensor response over an inflation-deflation cycle. We see that the resistance increases and decreases shortly before the 2 s inflation ends. When the pressure is held constant, the resistance decreases as the polymer relaxes (shaded in green). After the initial relaxation, the resistance remains constant as we hold the strain for 5 s. When we start deflation, the resistance increases (shaded in yellow) and then decreases as the strain on the sensor reduces. We have yet to determine the cause for the temporary increase in resistance, however, the effect is apparent and similar in all of our tests.

To characterize durability we tested 4 membranes once a day for 15 days (Fig. 3(e). The plot indicates several phenomena: 1) nonlinear increase in resistance with increasing stretch. We suspect that the non-linearity can be attributed to the relaxation effect combined with slight fluctuations in the inflation rate. 2) As the membrane deflates, the resistance first increases (largely due to the temporary increase in resistance discussed above), and then decreases with decreasing stretch. 3) Although the sensors generally behave the same, their raw response has significant variation. This occurs due to the manual and simple fabrication process; in Sec. IV-C we show how to account for these differences to perform shape reconstruction. 4) Finally, we see

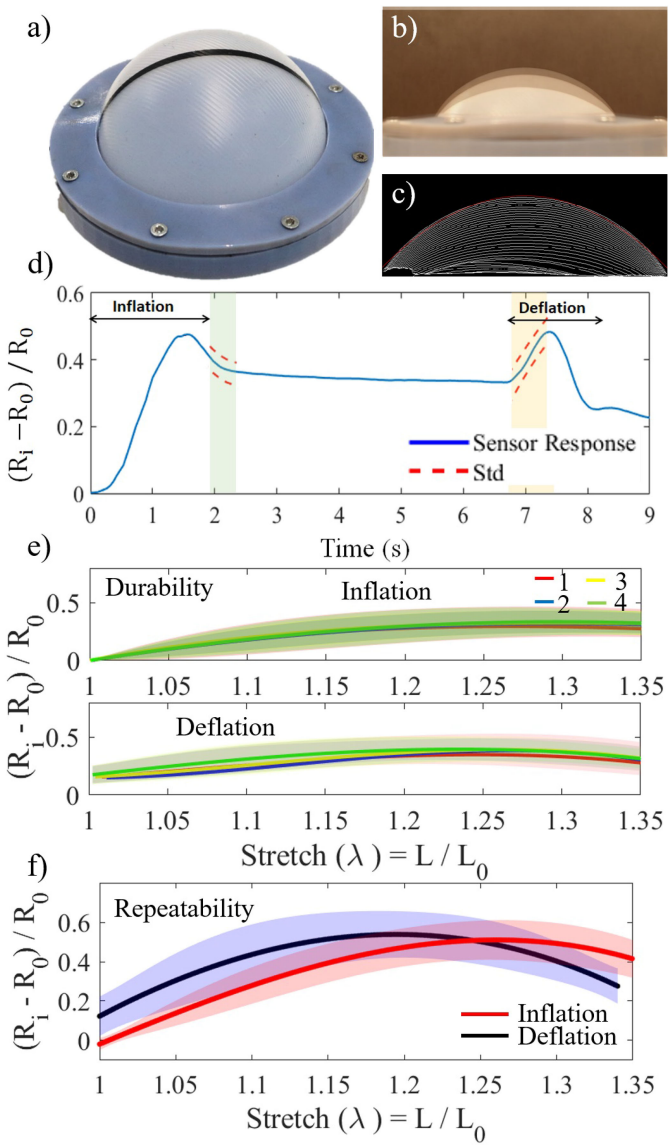

Fig. 3. (a) Setup used to characterize a single sensor. (b) Overlaid snapshots of a sensor membrane during inflation. (c) Matlab-generated plot to detect the membrane outline, i.e. membrane stretch, during inflation. (d) An example of the resistive response (blue) of a single sensor through one inflation-hold-deflation cycle. The red dashed line indicates the standard deviation over 15 days, during relaxation (green shaded region) and at the beginning of deflation (yellow shaded region). (e) Durability test of four separate sensors over 15 days. (f) Repeatability test of three sensors over 30 inflation cycles. The solid curve denotes the average resistance during inflation and deflation; the shaded regions are the standard deviations.

that each sensor is fairly durable with a relatively low average standard deviation of 0.11 (Ω/Ω) across all days.

Fig. 3(f) shows the signal response over 60 successive measurements, i.e. the repeatability of three sensors. Between each cycle we wait 2 min to mitigate effects from the visco-elastic relaxation. As the dome inflates, the resistance increases, reflecting the increase in stretch almost linearly. During deflation, the change in resistance is almost symmetric around the peak, and we use this symmetric property to identify the point of contact with objects as described in Sec. IV-C. Again, we see relatively low standard deviation over the 60 trials.

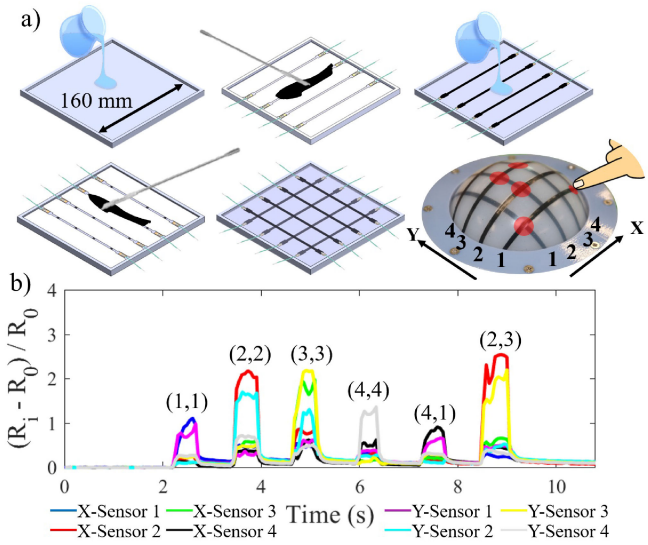

Fig. 4. (a) Fabrication procedure of a tactile grid. (b) Resistive response to perturbations; touch location can be pinpointed simply by looking for the sharpest increases in resistance.

III. Tactile Grid

The fabrication of the tactile grid sensor is graphically represented in Fig. 4. Using the same method described in Sec. II-B, we embed two perpendicular sets of 4 conductive channels in three layers of 160 mm × 160 mm × 1 mm substrate. We then constrain the membrane by an 85 mm-diameter circular clamp and inflate it with 50 mL of air. The entire process took less than 7 hours; 6 hours of which was for curing.

To demonstrate the use of the tactile grid, a user sequentially pressed on various regions of the inflated membrane. Specifically, we pressed on the six locations shown in Fig. 4(a-b). Note that because of the simple fabrication procedure, all sensor channels experience different initial resistance and behaviors. We counteract this, simply by subtracting their resistance at rest and normalizing by this amount. Here, we automatically determine which grid cell is being perturbed by looking at the two sensor channels with the sharpest increase in electrical resistance. Obviously, both the sensor and the data processing can be optimized depending on the specific application, which may include soft user interfaces, wearable devices, and more.

IV. Sensitive, Pneumatic Gripper

Although many recent papers discuss how soft robots may distinguish geometric shapes from one another [18], few touch on the challenge of actually measuring the object geometry [19]. The majority of these soft robots require active control and sophisticated analysis of the sensor so that it traces around the edge of the object. Other examples include soft sensors applied to augmented reality, where, e.g., haptic devices must give information about a virtual object's shape and texture [20]. Here, we describe a simple alternative to shape reconstruction.

A. Fabrication

Fig. 5 shows the steps needed to fabricate the soft gripper. Using the same method as fabricating a single carbon composite stretchable sensor, we embed 8 channels in a 160 mm × 115 mm × 2 mm substrate. We fold it into a cylindrical envelope and seal the rim with Ecoflex 00–10 mixture. This envelope is wrapped onto an acrylic cylinder (100 mm in height and 50 mm radius) to form an airtight gripper. We then insert a flexible tube for pneumatic actuation. Note, that the syringe pump was used for experimental ease, but the inflation could also have been done by hand. The total fabrication time for the gripper array was no more than 5 hours from start to completion.

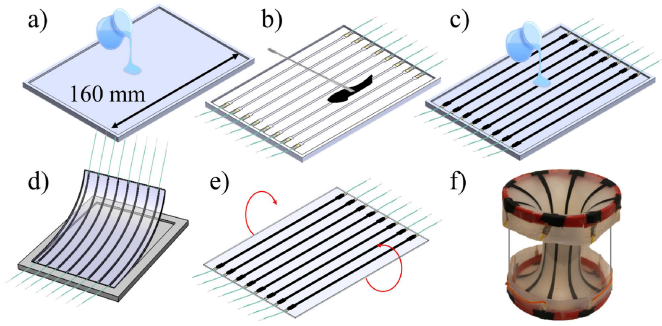

Fig. 5. Fabrication of the encapsulating sensor. (a) 25 g of Ecoflex 00–10 is poured into a rectangular mold to form a 1 mm thickness. (b) After the silicone has set, we laser cut a stencil with sensor patterns and place it on top of the silicone. The Carbon composite is spread across the laser cut mask and over the electrodes. (c) The mask is peeled off and a second layer of 25 g of Ecoflex 00–10 is poured. (d) The membrane is peeled off from its mold. (e) The membrane is folded along its long axis and 1 g of Ecoflex 00–10 is applied to join the two edges. (f) The encapsulating sensor is made by wrapping the edges around a Plexiglass cylinder and attaching a tube for actuation.The gripper is resting at ambient pressure.

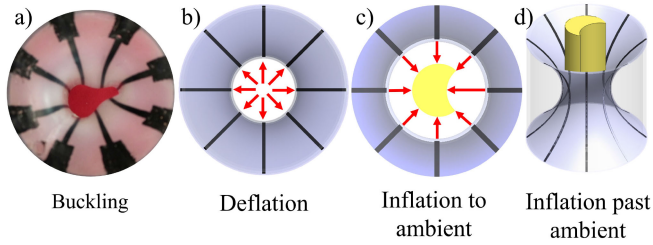

Fig. 6. (a) When the gripper is inflated past ambient, it risks buckling which complicates data processing. (b)-(d) Top and isometric views of the gripper as it measures an extruded (yellow) shape with convex and concave features. The red arrows indicate direction of motion.

B. Operation

We use a syringe pump to actuate the pneumatic gripper at the speed of 50 mL / s, causing a change in stretch at the same order of that used in the characterization of the single sensor (Sec. II-C). Note that using inflation alone would cause the material to buckle inwards, which would complicate sensor response and consequently the shape reconstruction (Fig. 6a). Instead, we avoid sensor buckling by only using the membrane under stretch. To sense the geometry of an encompassed object, we therefore conduct the following steps also shown in Fig. 6(b-d): (1) we deflate the gripper for 5 s to reach negative pressure, dilating the center of the gripper; (2) we hold a negative pressure for 5 s, during which we insert the object to be measured; (3) we

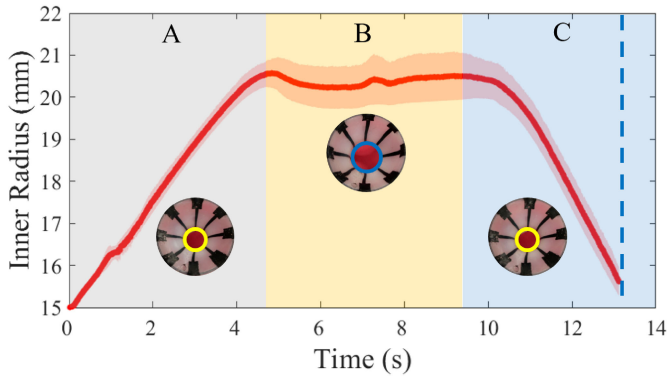

Fig. 7. Measurement of the inner radius of the gripper during a deflation(A)-hold(B)-inflation(C) cycle. The red curve shows the average of five cycles; the shaded region the standard deviation. The blue dashed line represents the point at which the gripper begins to buckle as shown in Fig. 6(a).

then inflate for 6 seconds, allowing the gripper to encompass the object fully. Pressure inside the gripper goes from ambient to negative (deflation and hold), to ambient and then positive pressure (inflation) subsequently.

The inner diameter of the gripper is 42 mm when fully deflated and is 30 mm when it reaches ambient. The range of the diameter of objects we can measure is therefore 30 mm to 42 mm. Fig. 7 shows how the inner diameter of the gripper changes during a sensing cycle. The radius of the opening increases and decreases almost linearly with time during deflation ($v_d = \Delta R/t = 1.54$ mm / s) and inflation ($v_i = \Delta R/t = 2.12$ mm / s). We use this property later when we estimate the shape of the object.

C. Shape Estimation

Next, we demonstrate the ability of the gripper to measure convex cylinders of different diameters, as well as a cylinder with a concave feature similar to a crescent moon shape. We use a motor-actuated syringe to keep the speed of the inflation at 50 mL / s, the same as the sensor characterization tests, such that we can expect similar behaviour of the membrane.

To measure the size of an encompassed cylinder, we simply measure the rate of change in resistance, ΔR, in each sensor channel at a rate of 136 samples per second. During ambient to inflation, the sensors experience increasing stretch which causes increasing resistance; however, as the sensors come into contact with the object, ΔR decreases significantly because the sensor no longer stretches and instead is compressed against the object surface. We automatically determine when ΔR changes. Specifically, we look at the readings during inflation (between 10 to 16 s), smooth the curve using a running average of nine samples, and then identify the peak in resistance, i.e. when the slopes of the smoothed resistance curves cross zero during inflation. We approximate the distance traveled by the sensor as the product of v_i and total inflation time. Using the speed of inflation estimated from the experiment in Fig 7, we can estimate the traversed distance of each channel. By focusing on when ΔR changes, rather than the actual resistance value, we bypass issues related to variations in sensor fabrication.

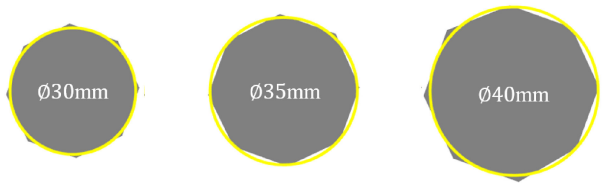

Fig. 8. Real (yellow) and reconstructed (gray shape) outlines for circular objects with varying diameter.

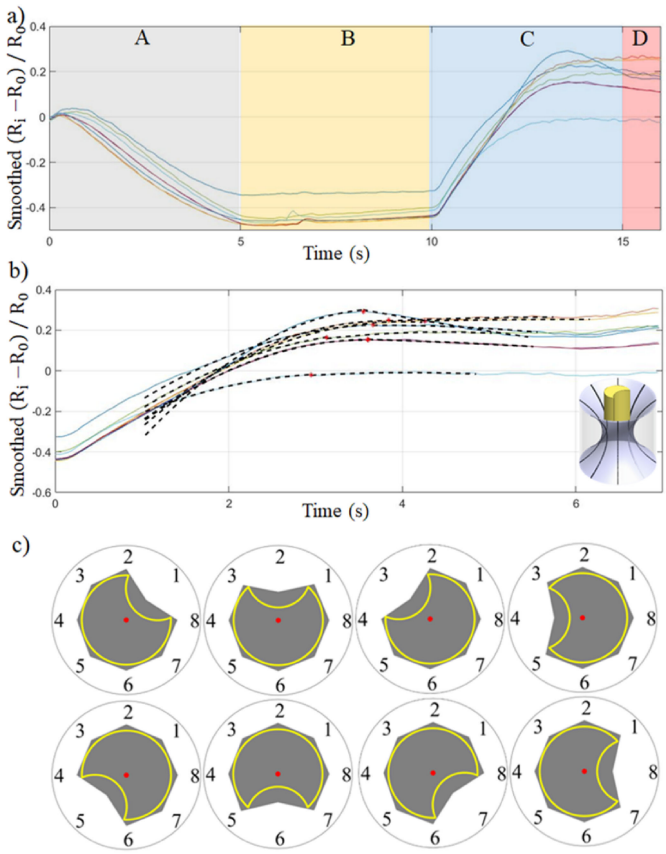

Fig. 9. (a) Sensor responses during a deflation (A)-hold (B)-inflation (C&D) cycle around a crescent moon shape. Membrane buckling occurs in (D) at the end of inflation. The object is inserted during the hold phase near 6 s. (b) By looking at the symmetric tendency around the peaks in the curve (marked in red), we can identify which sensor is located by the cavity. (c) Real (yellow) and reconstructed (gray shape) outlines of a concave object in eight different orientations.

We tested this simple technique on three cylinders of diameter 30 mm, 35 mm and 40 mm. The results are shown in Fig. 8. In these experiments, the mean error of the sensors is 0.7 mm, with a standard deviation of 0.65 mm and a maximum error of 1.48 mm. Note, that part of this error could be caused by a slight off-center placement of the object.

To demonstrate the ability of the technique to identify concave features in the crescent moon shape, we overinflate the gripper past ambient and estimate the position of the concavity. Fig. 9(a) shows an example of the response of all eight sensors during a full deflation-hold-inflation cycle. The resistance first drops as the gripper is deflated; then remains constant as

we hold the pressure; and finally increases as we inflate the gripper back to (and past) ambient pressure. During inflation, we notice two behaviors: the rate of resistance change drops in sensors that are in contact with the object; the rate of resistance change in sensors that have yet to reach the object exhibit a symmetric quadratic shape around its peak, which matches the rate of resistance change with stretch characterized in Sec. II-C. To find the latter automatically, we fit second-order polynomials to the data 0.25 seconds before and after the peaks (shown in Fig. 9b), and identify the one with the highest symmetry.

Fig. 9(c) shows the reconstructed shape of the crescent moon at 8 different orientations. The mean error of the sensors that are touching the crescent is 2.82 mm, with a standard deviation of 0.085 mm and a maximum error of 2.96 mm. Note that these sensors all overestimate the size of the object, but have a small standard deviation. The sensor accuracy could therefore be improved simply by subtracting this offset. In all eight tests, we are able to correctly identify the position of the cavity, however, these sensors have a much higher mean error of 7.26 mm. This happens because at 13 s the membrane starts bulging and buckling at the top and the bottom, before the sensor positioned by the cavity comes into contact with the object. Because we can only extrapolate the dimension of the object by how far the sensor has travelled towards the object, this makes the calculation erroneous. This issue could potentially be fixed by changing the thickness across the membrane so that the bulging occurs later.

Finally, although we only focus on rigid objects here, we hypothesize that the sensors may also work for soft or compliant objects, if their effective stiffness coefficient is more than or equal to that of a fully inflated gripper. A high stiffness coefficient will ensure that the encompassing the membrane of sensor will inflate around the object's perimeter and conform to its circumferential geometry.

V. Conclusion

In this paper, we showed a shape reconstruction technique based on simple, accessible fabrication methods, supported by customized mechanical implementations for simple control and processing. We demonstrated that its characteristics persist over multiple inflation cycles and as the sensor ages. Finally, we showed how it could be easily customized to fit the need of the user through a passive tactile array and a gripper for active shape recognition. The main contribution of our work is to make these sensors more easily adopted (and developed) by a wide range of researchers and users. The simple customized platforms we have shown, can be built upon to achieve better performance or behavior depending on the particular use case.

Acknowledgment

The authors would like to thank the support regarding the carbon composite pilot study from the MOE Key Laboratory of Material Chemistry for Energy Conversion and Storage, Huazhong University of Science and Technology, Wuhan, China.

References

[1] M. Amjadi, K. U. Kyung, I. Park, and M. Sitti, "Stretchable, skin-mountable, and wearable strain sensors and their potential applications: A review," *Adv. Functional Mater.*, vol. 26, pp. 1678–1698, 2016.

[2] L. Hines, K. Petersen, G. Z. Lum, and M. Sitti, "Soft actuators for small-scale robotics," *Adv. Mater.*, vol. 29, no. 13, 2017, Art. no. 1603483.

[3] Y.-L. Park, C. Majidi, R. Kramer, P. Berard, and R. J. Wood, "Hyperelastic pressure sensing with a liquid embedded elastomer," *J. Micromechanics Microengineering*, vol. 20, no. 12, Nov. 2010, Art. no. 125029.

[4] O. Atalay, A. Atalay, J. Gafford, and C. Walsh, "A highly sensitive capacitive-based soft pressure sensor based on a conductive fabric and a microporous dielectric layer," *Adv. Mater. Technologies*, vol. 3, 2018, Art. no. 1700237.

[5] E. Menard *et al.*, "Micro- and nanopatterning techniques for organic electronic and optoelectronic systems," *Chem. Rev.*, vol. 107, pp. 1117–1160, 2007.

[6] S. R. Forrest and M. E. Thompson, "Introduction: Organic electronics and optoelectronics," *Chem. Rev.*, vol. 107, pp. 923–925, 2007.

[7] X. Shi, C.-h. Cheng, and Y. Zheng, "An EGaIn-based flexible piezoresistive shear and normal force sensor with hysteresis analysis in normal force direction," *J. Micromechanics Microengineering*, vol. 26, 2016, Art. no. 105020.

[8] H. J. Choi, M. S. Kim, D. Ahn, S. Y. Yeo, and S. Lee, "Electrical percolation threshold of carbon black in a polymer matrix and its application to antistatic fibre," *Scientific Rep.*, vol. 9, pp. 1–12, 2019.

[9] M. Sumita, K. Sakata, S. Asai, K. Miyasaka, and H. Nakagawa, "Dispersion of fillers and the electrical conductivity of polymer blends filled with carbon black," *Polymer Bulletin*, vol. 25, pp. 265–271, 1991.

[10] J. H. Kong, N. S. Jang, S. H. Kim, and J. M. Kim, "Simple and rapid micropatterning of conductive carbon composites and its application to elastic strain sensors," *Carbon*, vol. 77, pp. 199–207, 2014.

[11] K. Y. Chun *et al.*, "Highly conductive, printable and stretchable composite films of carbon nanotubes and silver," *Nature Nanotechnol.*, vol. 5, pp. 853–857, 2010.

[12] S. Stankovich *et al.*, "Graphene-based composite materials," *Nature*, vol. 442, pp. 282–286, 2006.

[13] H. Pang, T. Chen, G. Zhang, B. Zeng, and Z. M. Li, "An electrically conducting polymer/graphene composite with a very low percolation threshold," *Mater. Lett.*, vol. 64, pp. 2226–2229, 2010.

[14] L. Yue, G. Pircheraghi, S. A. Monemian, and I. Manas-Zloczower, "Epoxy composites with carbon nanotubes and graphene nanoplatelets - Dispersion and synergy effects," *Carbon*, vol. 78, pp. 268–278, 2014.

[15] M. R. Loos, J. Yang, D. L. Feke, and I. Manas-Zloczower, "Effect of block-copolymer dispersants on properties of carbon nanotube/epoxy systems," *Composites Sci. Technol.*, vol. 72, pp. 482–488, 2012.

[16] J. Shintake, V. Cacucciolo, D. Floreano, and H. Shea, "Soft robotic grippers," *Adv. Mater.*, vol. 30, no. 29, 2018, Art. no. 1707035.

[17] Y. S. Ye *et al.*, "Biocompatible reduced graphene oxide sheets with superior water dispersibility stabilized by cellulose nanocrystals and their polyethylene oxide composites," *Green Chemistry*, vol. 18, pp. 1674–1683, 2016.

[18] B. S. Homberg, R. K. Katzschmann, M. R. Dogar, and D. Rus, "Haptic identification of objects using a modular soft robotic gripper," in *Proc. IEEE Int. Conf. Intell. Robots Syst.*, 2015, pp. 1698–1705.

[19] B. Ward-Cherrier *et al.*, "The tactip family: Soft optical tactile sensors with 3D-printed biomimetic morphologies," *Soft Robot.*, vol. 5, pp. 216–227, 2018.

[20] C. Larson, J. Spjut, R. Knepper, and R. Shepherd, "A deformable interface for human touch recognition using stretchable carbon nanotube dielectric elastomer sensors and deep neural networks," *Soft Robot.*, vol. 6, pp. 611–620, 2019.